Korean J. Chem. Eng., 37(10), 1669-1679 (2020)
DOI: 10.1007/s11814-020-0571-9

pISSN: 0256-1115
eISSN: 1975-7220

Electrooxidation of single-carbon molecules by nanostructured Pd-decorated spongy ceria

Zahra Yavari*,,†, Mahdi Shafiee Afarani***, Amir Masoud Arabi****, and Meissam Noroozifar*****,†**

*Department of Chemistry, University of Sistan and Baluchestan, P.O. Box 98135-674, Zahedan, Iran
**Renewable Energies Research Institute, University of Sistan and Baluchestan, Zahedan, Iran
***Department of Materials Engineering, Faculty of Engineering, University of Sistan and Baluchestan, Zahedan, Iran
****Department of Inorganic Pigments and Glazes, Institute for Color Science and Technology (ICST), Tehran, Iran
*****Department of Physical and Environmental Sciences, University of Toronto Scarborough 1265 Military Trail, Toronto, Ontario, M1C 1A4, Canada

(*Received 24 December 2019 • Revised 9 May 2020 • Accepted 11 May 2020*)

Abstract−Solution combustion synthesis is proposed to fabricate spongy ceria by using two different fuels for combustion: glycine and urea. As-prepared samples are labeled as SCO_{Gl} and SCO_{Ur}. The acid-base properties of the cavities and surfaces of specimens are determined by measuring the pH of zero charges. Both SCO_{Gl} and SCO_{Ur} powders are decorated by the nanostructured Pd (NSPd) by the wetness incorporation. The NSPd-SCO_{Gl} and NSPd-SCO_{Ur} represent the high mass current density than NSPd as non-supported palladium for the electrooxidation of single-carbon molecules: methanol, formaldehyde and formic acid. The results show that the NSPd-SCO_{Gl} and NSPd-SCO_{Ur} are exceptional heterogeneous catalysts. The SCO as the support with porous structural network has been affected considerably on the electrochemical surface area, dispersion, and durability of NSPd. On the other hand, it can be effective for removing the poisoning species of the electrooxidation of single-carbon molecules on NSPd through the lattice oxygen, and the activation of an oxidation-reduction cycle between the high and low chemical valences of cerium, leading to improve the electrocatalytic efficiency of NSPd. Finally, it is confirmed the conversion of methanol to formaldehyde, and then to formic acid during electrooxidation by using cyclic voltammetry studies.

Keywords: Single-carbon Molecules, Solution Combustion Synthesis, Methanol, Electrocatalyst, Cerium (IV) Oxide

INTRODUCTION

The electrooxidation of organic compounds is widely connected with the progress of fuel cells and the electrochemical sensors [1-4]. It is an electrocatalytic reaction proceeding over electron transfers and is intricate *via* the molecule adsorption on the surface of heterogeneous catalyst and creation of poisoning intermediate. Such reactions are great electrocatalyzed on noble metals [5,6] with great ability toward dehydrogenation molecules, as well as one providing oxygen species [7]. Succinctly, it may be essential to progress the transport kinetics of electron in electrocatalysts to increase the electrocatalysts activity.

Currently, the support materials are considered [8-10], because they restrain the agglomerating noble metals and create a stable structure with high surface area efficiently; also, they have encouraging electronic and geometric properties to advance the interaction among particles of noble metals and electrode surface, resulting in the improvement of electrocatalytic abilities [11]. To improve the dispersion of noble metals, carbon materials are frequently studied as electrocatalyst supports [12,13]. Despite the high conduction coefficient of the carbon structures, current electrocatalysts still suffer from low utilization of noble metal, incomplete mass transportability, and the confined electrochemical stability of the carbon-based supports [14]. Hence, due to different properties like slight thermal conductivity, great thermal stability, and significant resistance to degradation for ceramic materials [15], they have attracted much attention to be available support for catalytic materials. The structural stability and feasibility of charge propagation are two key factors for the dispersion of noble metals in electrocatalysts in the support selection. Up to now, some ceramic structures are utilized in the catalytic electrooxidation of organic compounds, such as WO_3 [16], TiO_2 [7,17], SnO_2 [18,19], SiO_2 [20], $Ti_{0.5}Cr_{0.5}N$ [21] and $NiCo_2O_4$ [22]. Electrocatalytic materials with diverse morphologies or structures possess distinct behaviors. Therefore, materials with similar composition and different morphologies have been studied in the literature [23-25]. In the recent decade, porous materials have attracted more consideration owing to their specific skeletal feature, superior surface area, and the controllable cavity size. Also, they supply a short pathway to transport electrons and ions, consequently leading to rapid process kinetics. On the other hand, it is confirmed the efficiency of transition metal oxides is primarily managed through electrochemical behavior and kinetic characteristic of the active materials [26].

Although there are numerous literature researches on electro-catalysts introduction in the fuel cell, further study is essential. CeO_2 has been successfully employed as a compound of the catalytic com-

†To whom correspondence should be addressed.
E-mail: z_yavari@chem.usb.ac.ir, m.noroozifar@utoronto.ca

posite in volatile organic compound oxidation [27], selective alcohol oxidation [28], and ethanol steam reforming [29]. There are many investigations on the synthesis of CeO_2 powders with different methods such as precipitation [30], combustion [31], sol-gel [32], and hydrothermal [33] synthesis.

The aim of this paper was the fabrication of cerium (IV) oxide as spongy support by a novel approach. Solution combustion synthesis was selected as an appropriate method because of its easy-eco and fast process consuming low-cost starting materials [34]. The spongy ceria was synthesized by using two different fuels for combustion: glycine and urea. The samples are denoted as SCO_{Gl} and SCO_{Ur}. In the following, the wetness incorporation of spongy ceria was carried out with an aqua mixture of palladium precursor and deacetylchitin as an adhesive agent. Then a fast chemical reduction was performed to reach nanostructured Pd (NSPd). The electrocatalytic activity of as-fabricated composites was assessed toward electrooxidation of single-carbon molecules as feed in the polymeric fuel cells--methanol, formaldehyde, and formic acid--*via* electrochemistry techniques.

MATERIALS AND METHODS

1. Characterization Instruments

X-ray diffraction (XRD) was considered for the structural characterization of samples by using Bruker, Advanced D8. Molecular characterizations utilized Fourier-transform infrared spectroscopy (FT-IR, Bruker Tensor II). The microstructure of samples was observed by scanning electron microscopy (SEM, KYKY EM3900). The surface area was measured with Brunauer-Emmett-Teller (BET) theory using nitrogen adsorption at 77 K via surface area analysis, and adsorption isotherms were determined with a BELSORP-mini II instrument. Energy-dispersive X-ray spectroscopy (EDXS) was employed to control the composition of the mentioned electrocatalyst. Field emission scanning electron microscopy (FESEM) was selected to inspect the morphology of the NSPd/S-CeO_2. EDXS and FESEM samples were, respectively, evaluated by using the SAMX electron microscope and MIRA3 TESCAN. A SAMA 500 Electroanalyzer (SAMA Research Center, Iran) was used for electrochemical investigations. An auto-lab PGSTAT 128N (EcoChemie, Netherlands) potentiostat/galvanostat with NOVA 2.1 carried out electrochemical impedance spectroscopy (EIS) examination. To determine the acid-base property of the spongy ceria, a specific amount of CeO_2 powder was suspended in 10 ml (5×10^{-3} M) KNO_3 aqueous solution during 60 min N_2 bubbling to avoid any contamination from the presence of carbon dioxide in the atmosphere. After the pH of the mixture was regulated at 12 by 0.1 M NaOH, the suspension was titrated with 0.1 M HNO_3. The point data were recorded after the pH became stable by using a Metrohm pH meter, model 744.

2. Experimental Procedure

CeO_2 nanocrystallite structures were synthesized by solution combustion synthesis using propellant stoichiometry for glycine and urea fuels based on the following reactions:

$$6\ Ce(NO_3)_3{\cdot}6H_2O+10\ C_2H_5NO_2 \rightarrow 3\ CeO_2+20\ CO_2+61\ H_2O+14\ N_2 \quad (1)$$

$$2\ Ce(NO_3)_3{\cdot}6H_2O+5\ CH_4N_2O \rightarrow CeO_2+5\ CO_2+22\ H_2O+8\ N_2 \quad (2)$$

Cerium nitrate hexahydrate ($Ce(NO_3)_3{\cdot}6H_2O$, Merck) was as oxidizer staring material. Glycine ($C_2H_5NO_2$, Merck) and urea (CH_4N_2O, Merck) were used as fuels for combustion. In each solution, 1.320 g oxidizer and a known amount of fuel (0.380 g glycine and 0.457 g urea) with certain concentrations (with molar ratio of oxidants to fuel equal to 1) were dissolved in 10 ml of deionized water at 300 °C and adjusted pH (respectively, 4.5 and 5 for solution containing glycine and urea). The resultant solution was mixed under magnetic stirring at about 150 °C to reach a thick hydro-gel. The gained gel was heated at 300 °C until the combustion process happened, and yellowish nano crystallite powder was prepared in the spongy structure and denoted as SCO_{Gl} and SCO_{Ur}.

The wetness incorporation of 3 mg SCO_{Gl} and/or SCO_{Ur} was carried out with aqueous solution containing $PdCl_4^{2-}$ described as follows: 25 µl 37% HCl (Merck)+1 ml doubly distilled water+5 mg $PdCl_2$ (Sigma-Aldrich)+2 ml of 1.7 mg·l^{-1} deacetylchitin (Fluka) solution in the dilute solution of ethanoic acid (Merck). A fast chemical reduction was performed *via* the addition of 50 µl of 100 mg·ml^{-1} of $NaBH_4$ (Merck) solution and the final product denoted as NSPd. As-prepared nanocomposites were denoted as NSPd-SCO_{Gl} and NSPd-SCO_{Ur}. It is known that the performance of the electrocatalyst is influenced by various factors: morphology, palladium loading, and synthesis approach. Hence, to better investigate the support effect on efficiency, the NSPd as a non-supported catalyst was synthesized via a similar procedure.

3. Electrochemical Measurements

An electrochemical cell was used to conduct cyclic voltammetry, controlled potential coulometry, and potentiodynamic polarization analysis. A Pt wire served as the counter electrode. The silver/silver chloride (Ag/AgCl) or mercury/mercury oxide (Hg/HgO) reference electrodes served as the reference electrodes by pH of electrolyte. A glassy carbon (GC, ~0.0314 cm^{-2} surface areas) electrode was pre-prepared by the described method in [35]. Then, to prepare the working electrode, 10 µl catalytic composite was spread and dried on an activated GC electrode.

The CO electrooxidation on the modified electrodes was assessed in the following way: CO was adsorbed at a known potential (~0.05 V) for 10 min. Subsequently, nitrogen gas was used to remove dissolved CO for 25 min. The potentials scan was recorded.

Electrochemical impedance measurements covered a frequency region of 0.1 Hz to 100 kHz in 4.5 mM $[Fe(CN)_6]^{3-/4-}$ mixed in 0.1 M potassium chloride.

RESULTS AND DISCUSSION

1. Structural Characteristics

Fig. 1(A) displays XRD patterns of samples produced with glycine and urea fuels. As shown, CeO_2 (01-081-0792), the major phase, was detected no minor crystalline phase. Likewise, no considerable change could be seen in the structure of synthesized powders. The broadening of CeO_2 peaks was attributed to the nanocrystalline essence of samples with an average crystallite dimension of close to 26 and 13 nm for powders, which were, respectively, synthesized with glycine and urea fuels. It is due to the high rate of combustion reaction which crystallites cannot grow, considerably. In comparison to SCO_{Ur}, the SCO_{Gl} represented narrower and stron-

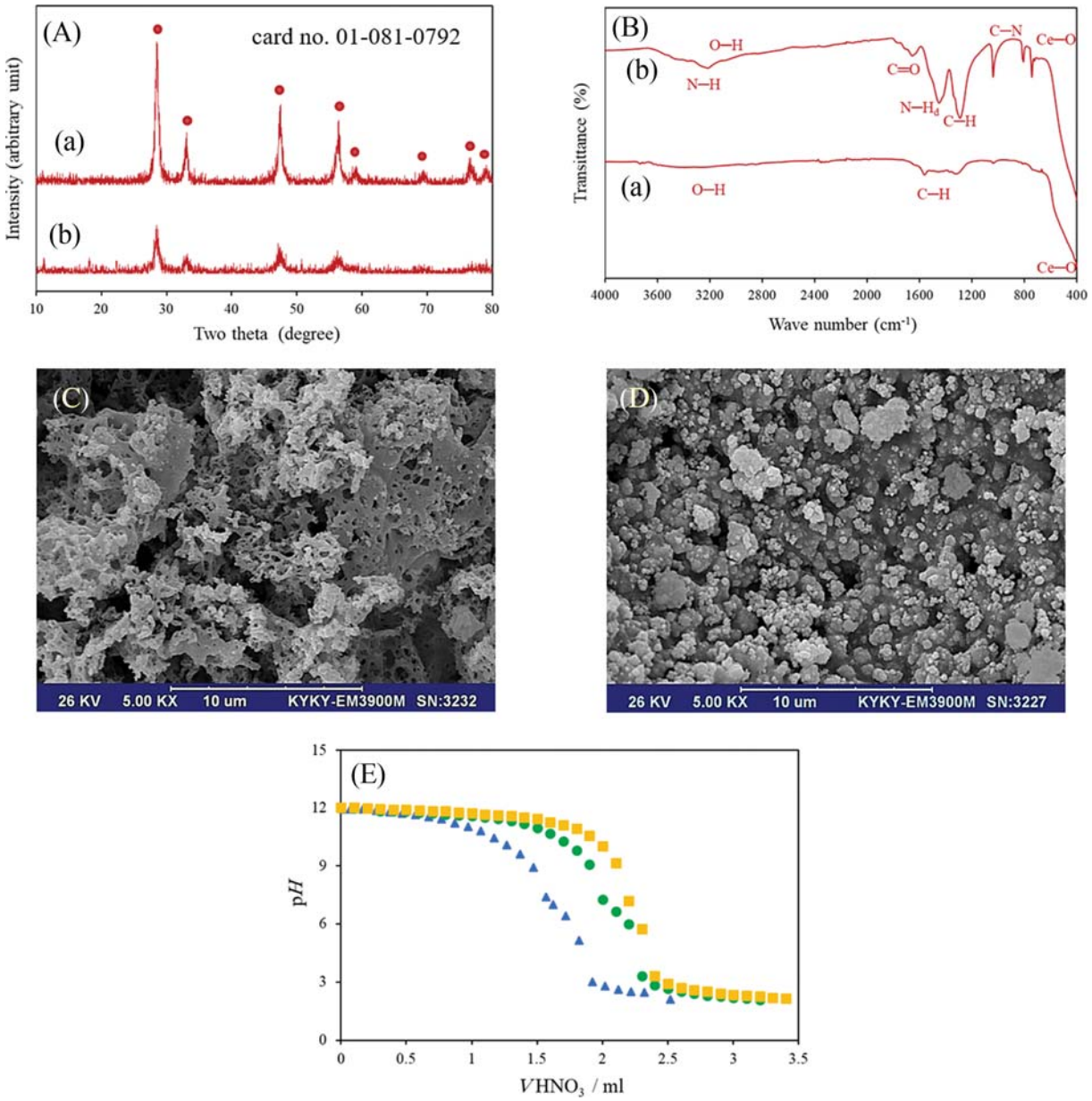

Fig. 1. (A) XRD patterns and (B) FT-IR spectra for (a) SCO_{Gl} and (b) SCO_{Ur} nano-crystallite powders, SEM micrographs of (C) SCO_{Gl} and (D) SCO_{Ur}, and (E) the curves of (△) blank, (○) SCO_{Gl} and (□) SCO_{Ur} titration to determine PZC value.

ger peaks in the XRD patterns. It seems that combustion reaction with glycine released more heat value and caused the formation of CeO_2 nanostructured with more crystallinity. Thus, the combustion reaction with urea was weaker than glycine one and could not completely transform amorphous gel-like precipitate to nanocrystalline CeO_2 particles.

Fig. 1(B) shows the FT-IR spectra of samples synthesized with glycine and urea fuels. In Fig. 1(B(a)) and (b) spectra, the peak about 2,000-3,400 cm^{-1} was associated to O-H stretching vibration of H_2O in the samples [36] and the absorption bands at 1,300, and 1,600 cm^{-1} were ascribed to the bending vibration of C-H stretching [36], which might be due to unreacted fuel components. Also, the band less 800 cm^{-1} was due to the Ce-O stretching [30]. In Fig. 1(B(b)) spectrum, the C=O, and C-N stretching was, respectively, revealed at 1,680 and 1,100 cm^{-1}. Also, the N-H stretching and deformation appeared at 3,460 cm^{-1} and 1,625 cm^{-1}, respectively [37]. As mentioned, urea combustion is less completed than glycine. So, peaks attributed to remained organic components have higher intensities.

Fig. 1(C) and (D) illustrates SEM micrographs of SCO_{Gl} and SCO_{Ur}, respectively. As expected, the large amount of exhausted gasses during the combustion process and high-temperature reaction led to a porous and highly agglomerated microstructure for both nano crystallite powders. In comparison to urea, the use of glycine fuel caused more sponge-like morphology particles. Likewise, in the samples synthesized with urea fuel, some remaining gel-like amorphous products together with nanoparticles can be observed (Fig. 1(D)), which is due to a stronger combustion reaction of glycine fuel than urea fuel.

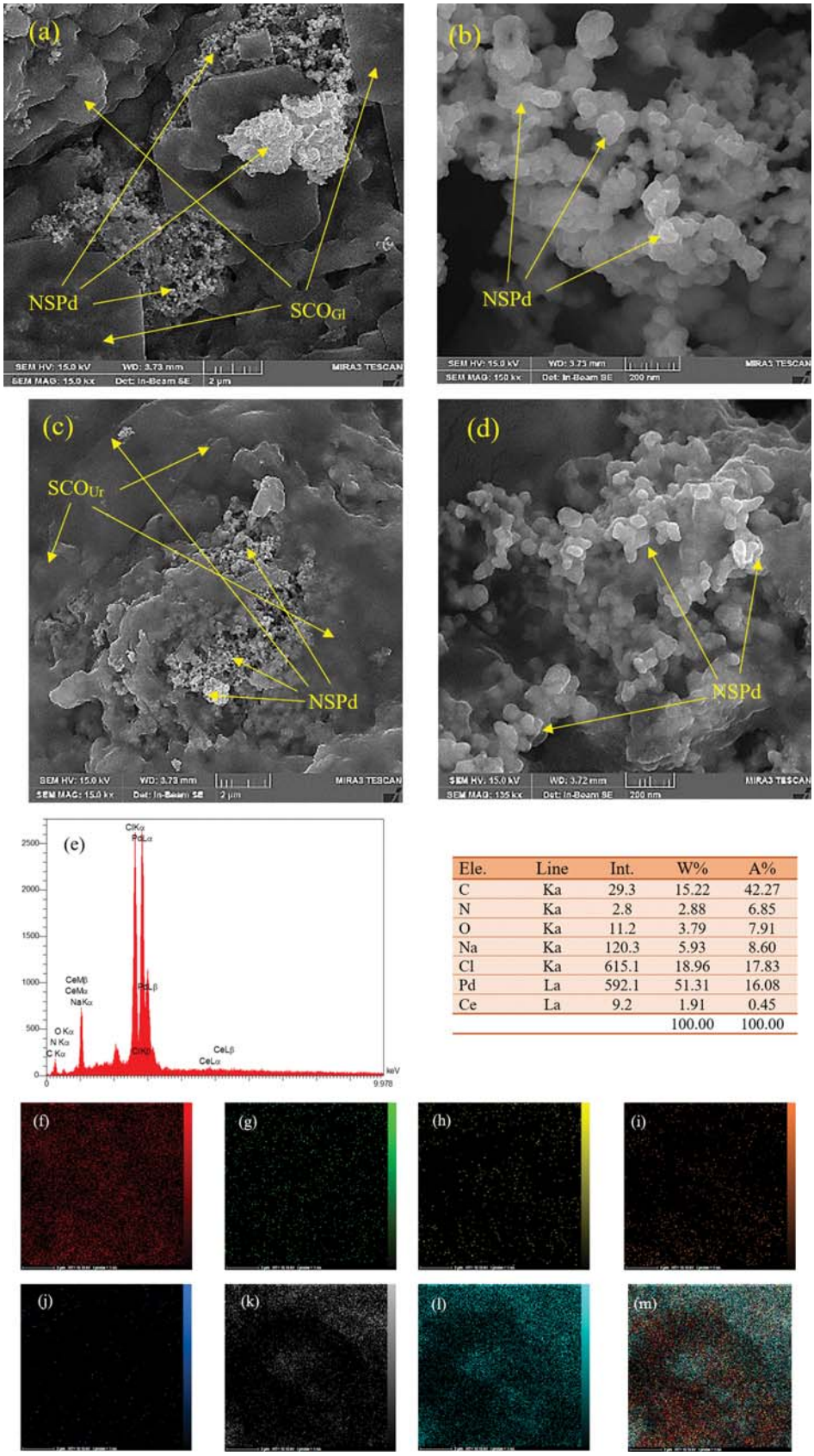

Ele.	Line	Int.	W%	A%
C	Ka	29.3	15.22	42.27
N	Ka	2.8	2.88	6.85
O	Ka	11.2	3.79	7.91
Na	Ka	120.3	5.93	8.60
Cl	Ka	615.1	18.96	17.83
Pd	La	592.1	51.31	16.08
Ce	La	9.2	1.91	0.45
			100.00	100.00

Fig. 2. FESEM images of ((a) and (b)) NSPd-SCO$_{Gl}$ and ((c) and (d)) NSPd-SCO$_{Ur}$ with 2 μm and 200 nm magnifications, respectively; (e) EDXS (Inset: elemental analysis) and elemental mapping: (f) palladium, (g) cerium, (h) oxygen, (i) carbon, (j) nitrogen, (k) natrium, (l) chlorine, and (m) Pd-Ce-O-C-N-Na-Cl merged for NSPd-SCO$_{Gl}$.

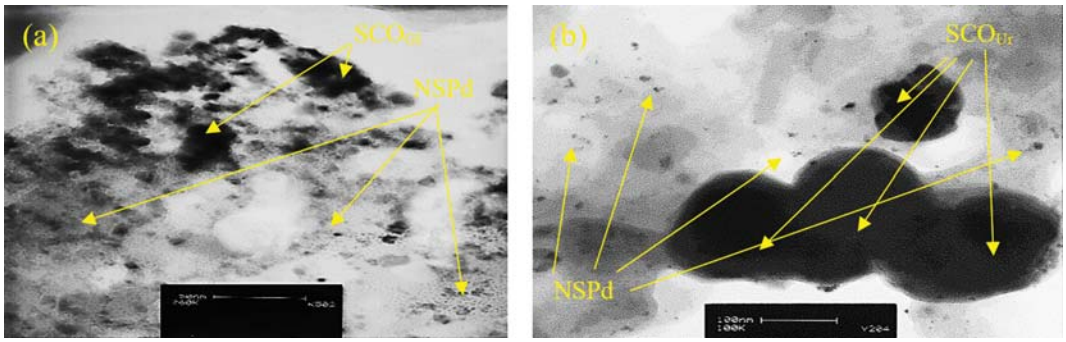

Fig. 3. TEM images of (a) NSPd-SCO$_{Gl}$, and (b) NSPd-SCO$_{Ur}$ electrocatalysts.

The surface areas of SCO$_{Gl}$ and SCO$_{Ur}$ nanopowders were estimated using BET analysis as 39.21 and 8.48 $m^2 \cdot g^{-1}$, respectively. As expected, SCO$_{Gl}$ with more sponge-like morphology (Fig. 1(C)) caused the dramatically greater surface area.

The support cavities nature as an intensive property can control the electronic factors of the active sites, while can be obtained *via* the evaluation of surfaces and cavities acid-base attributes of support in an aqueous medium. The acid-base property of the oxide cavities and surfaces is determined by measuring the pH of zero charges (PZC). It is a criterion of Lewis acidity, while it can be evaluated through the potentiometric acid-base titration. The PZC of ceramic support was measured to determine the intersection of the titration curves in the absent (blank solution) and presence of SCO$_{Gl}$ and SCO$_{Ur}$ (Fig. 1(E)) and were found to be 11.90 and 11.95, respectively. They are much more than those reported in the literature [38]. It seems that the PZC value for supports can be an influence on the electrocatalytic activity. The acidity of the cavities and surfaces OH group and also its bond strength to the active sites of cerium (Ce-OH) in CeO_2 decreases with increasing of the PZC value. Therefore, the higher PZC will cause more reactivity of adsorbed OH because of the weakening of its bond strength.

The morphology of NSPd-SCO$_{Gl}$ and NSPd-SCO$_{Ur}$ composites was probed by FESEM images displayed in Fig. 2(a) to 2(d). Based on Fig. 2(a) and 2(c), it was demonstrated the embedment of Pd crystals into ceria cavities for both supports. Fig. 2(b) and 2(d) represent low magnification FESEM images of NSPd-SCO$_{Gl}$ and NSPd-SCO$_{Ur}$; depicting the decoration of NSPd with sizes less than 100 nm on the surface and into cavities of the SCO$_{Gl}$ and SCO$_{Ur}$ supports, uniformly. It may be inferred the size and dispersion of nanoparticles for NSPd-SCO$_{Gl}$ were better than NSPd-SCO$_{Ur}$.

Hence, EDXS and elemental mapping were, respectively, carried out to study the chemical arrangements and the elemental distribution in NSPd-SCO$_{Gl}$, illustrated in Fig. 2(e) and (c). The EDXS pattern of NSPd-SCO$_{Gl}$ in Fig. 2(e) confirmed the presence of palladium, cerium, and oxygen. The elements of carbon and nitrogen were related to deacetylchitin polymer. Also, there were a few percentages of sodium and chlorine elements from the reduction reaction. The achieved results from EDXS are reported in Table inset Fig. 2(e). Fig. 2(f) through 2(m) display the elemental mapping of palladium, cerium, oxygen, carbon, nitrogen, natrium, and chlorine, respectively. Fig. 2(m) proves the excellent distribution of NSPd on SCO$_{Gl}$ support, which can lead to improving the electrocatalytic activity.

Fig. 3 represents the TEM images of NSPd-SCO$_{Gl}$ and NSPd-SCO$_{Ur}$ electrocatalysts. As seen in Fig. 3, palladium was synthesized as a nanostructure with a diameter of less than 100 nm. This is due to the rapid decrease in palladium ions with a strong reducing agent ($NaBH_4$). Also, the sponge support can prevent the accumulation of palladium particles.

2. Electrocatalytic Performance

The electro-oxidation of organic compounds is essential, such as alcohols, aldehydes, or carboxylic acids as fuel instead of hydrogen in a polymeric fuel cell. Methanol has received the most attention due to simple structure, high energy density, and easy industrial production. Nevertheless, issues such as low boiling point, crossover, environmental hazards, and health and neurotoxicity risk of methanol are inescapable. Formaldehyde as a small molecule can be a favorite subject in the development of polymeric fuel cell technology. Formic acid as an emerging fuel can alleviate some drawbacks of direct methanol fuel cells. Although this compound has lower energy density in comparison with the other competitors, it has an easy dissociation, flat crossover rate (due to repulsive force between the membrane and formate anions) and high safety. Hence, the process of single-carbon molecule electrooxidation on the modified electrodes was assessed utilizing chronoamperometry (CA) and CV techniques.

Fig. 4 shows the CA plots related to the electrooxidation of methanol, formaldehyde, and formic acid on GC/NSPd, GC/NSPd-SCO$_{Gl}$, and GC/NSPd-SCO$_{Ur}$ electrodes. The condition and the and results are defined in Table 1. The area under the CA curve represents the electrical charge transferred between the single-carbon molecule and the working electrode. An overview shows the presence of support increases this quantity for all three oxidation processes. According to Table 1, the data comparison to NSPd as the non-supported palladium represents that support structure improved the electrochemical stability for the single-carbon molecules electrooxidation. On the other hand, the GC/NSPd-SCO$_{Gl}$ illustrates more electric charge transferred compared to GC/NSPd-SCO$_{Ur}$ electrode at the same potential. The more active sites available on the GC/NSPd-SCO$_{Gl}$ electrode help to the higher surface area, the more storage of electrooxidized species, and more effortless charging of the double layer. There was an apparent fast current decay for both electrocatalysts at the beginning of the CA. It was due to the creation of intermediates, which were produced during the electroo-

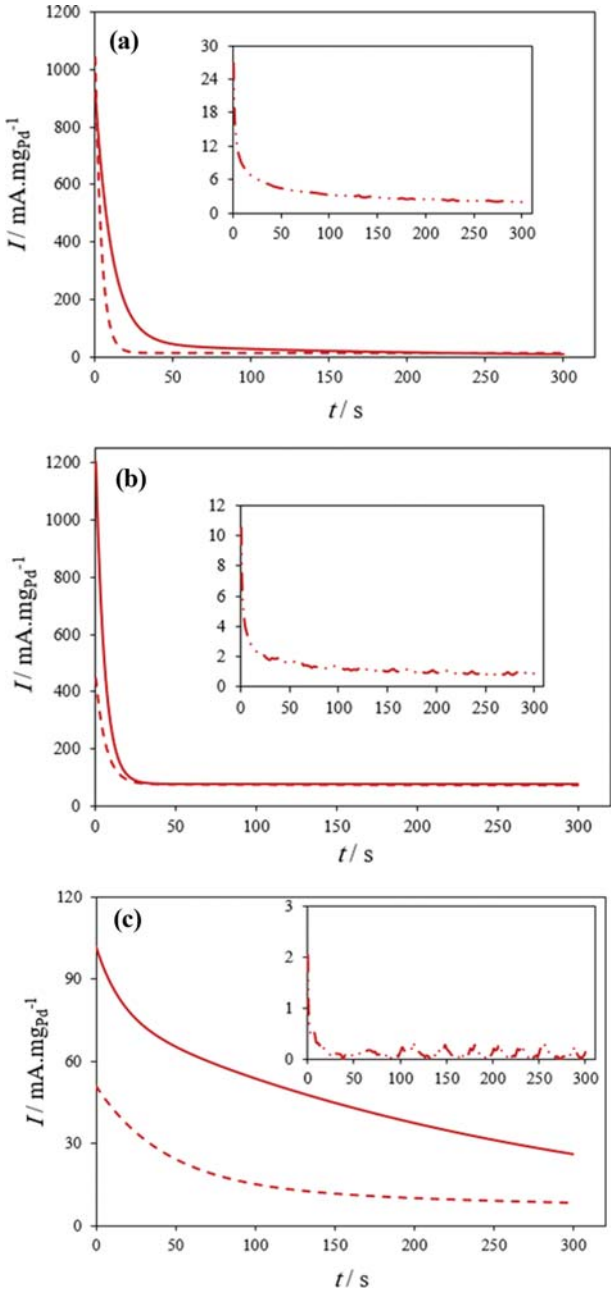

Fig. 4. CAs of (a) 0.80 M Methanol, (b) 0.18 M Formaldehyde, and (c) 0.51 M Formic acid, electrooxidation on (—) GC/NSPd-SCO$_{Gl}$, (----) GC/NSPd-SCO$_{Ur}$, (-···-) GC/NSPd electrodes at 0.1 V.

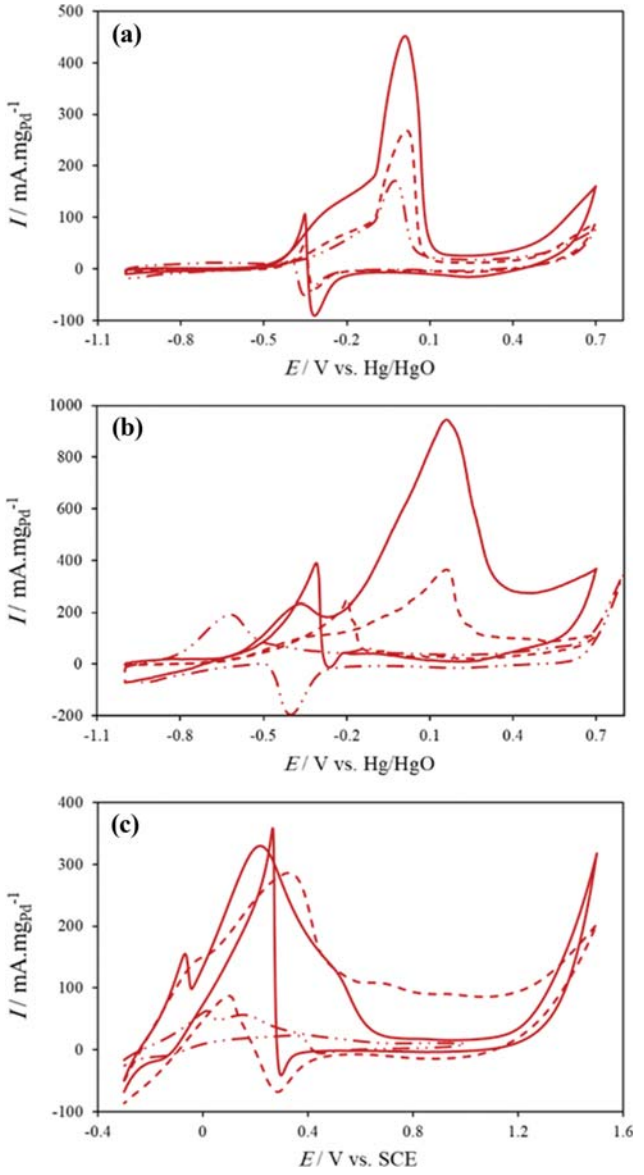

Fig. 5. CVs of (a) 0.32 M Methanol, (b) 0.18 M Formaldehyde, and (c) 0.09 M Formic acid, electrooxidation on (—) GC/NSPd-SCO$_{Gl}$, (----) GC/NSPd-SCO$_{Ur}$, (-···-) GC/NSPd electrodes at 0.05 V·s^{-1} sweep rate.

xidation, and subsequently were adsorbed on the surface of electrocatalyst, poisoning the active site. The durability and electrocatalytic activity of NSPd, NSPd-SCO$_{Gl}$ and NSPd-SCO$_{Ur}$ can be inferred from the beginning currents ($I_{(t=0\,s)}$) and the plateau currents ($I_{(t=300\,s)}$). The turnover number (TON) and turnover frequency (TOF) were obtained according to [39] and [40], respectively (See Table 1). Both quantities determine the efficiency of NSPd, NSPd-SCO$_{Gl}$, and NSPd-SCO$_{Ur}$ toward single-carbon molecules electrooxidation. According to Table 1, TON and TOF for GC/NSPd-SCO$_{Gl}$ are higher than GC/NSPd and GC/NSPd-SCO$_{Ur}$ for all three molecules. An intermediate metal base supports like CeO_2 was the promoter agent for the dehydrogenation as the initial step of oxidation of single-carbon molecules due to their multi-oxidative state, because it can be desirable to create an oxidation-reduction cycle among the high and low valences. It seems that the surface oxygen of ceria in the proximity of NSPd be effective in activating the oxidation process. Meanwhile, the porous structure of CeO_2 in SCO$_{Gl}$ and SCO$_{Ur}$ prevents sintering, dissolution, and aggregation of NSPd. So that, the SCO$_{Gl}$ as more porous support provides an upper area for the electrooxidation of a higher number of molecules at the NSPd catalyst surface than SCO$_{Ur}$.

Fig. 5 displays the CV curves related to the molecules electrooxidation on NSPd, NSPd-SCO$_{Gl}$, and NSPd-SCO$_{Ur}$. The concentration, electrolyte, reference electrode, and potential range are defined

Table 1. The electrochemical data as estimated from CA plots for the electrooxidation on the modified electrodes

Fuel	Electrocatalyst	C (M)	Electrolyte	$I_{(t=0\,s)}$ ($mA \cdot mg^{-1}_{Pd}$)	$J_{(t=300\,s)}$ ($mA \cdot cm^{-2}$)	n[a*]	TON[b*]	TOF[c]$\times 10^{-3}$* (s^{-1})
Methanol	NSPd-SCO_{Gl}	0.80	1 M NaOH	1,063.08	2.11	6	1.45	4.83
	NSPd-SCO_{Ur}			921.69	0.53		0.36	1.20
	NSPd			26.85	0.01		0.006	0.02
Formaldehyde	NSPd-SCO_{Gl}	0.43	1 M NaOH	1,594.48	16.18	4	16.71	55.69
	NSPd-SCO_{Ur}			509.66	18.05		18.65	62.16
	NSPd			10.51	0.03		0.030	1.00
Formic acid	NSPd-SCO_{Gl}	0.85	0.1 M H_2SO_4	113.95	6.60	2	13.64	45.46
	NSPd-SCO_{Ur}			76.69	2.13		4.40	14.67
	NSPd			2.02	0.23		0.475	1.58

[a]n=the number of transferred electrons during oxidation of one mole analyte.

[b]$TON = \frac{J \times N_A}{n \times F \times m_{Pd}}$ {N_A=Avogadro number, F=Faraday constant and m=atomic density of surface ($m_{Pd\,(111)}=1.51\times10^{+15}$ atoms number$\cdot cm^{-2}$)}

[c]$TOF = \frac{TON}{t}$ {t=300 s}

*If the oxidation reaction be complete (to produce CO_2), and not partial oxidation.

Table 2. Comparison of the electrooxidation to literature

	Catalyst	[C] (M)	Electrolyte	Ref. Ele.	E_{onset} (V)	E_f (V)	I_f	E_b (V)	I_b	Ref.
Methanol	PtRu/MWCNTs	2.00	0.1 M H_2SO_4	Ag/AgCl	+0.02	+0.6	39.82 $mA \cdot mg^{-1}$	+0.38	20.67 $mA \cdot mg^{-1}$	[42]
	Pt_p/C	0.50	0.5 M H_2SO_4	Ag/AgCl	Un-R*	+0.75	167 $mA \cdot mg^{-1}$	+0.5	152 $mA \cdot mg^{-1}$	[43]
	PdNPs-CH	0.80	1.0 M KOH	Hg/HgO	−0.67	−0.14	4.77 $mA \cdot cm^{-2}$	−0.30	1.71 $mA \cdot cm^{-2}$	[44]
	NSPd-SCO_{Gl}	0.32	1.0 M NaOH	Hg/HgO	−0.96	+0.01	452.11 $mA \cdot mg^{-1}$	−0.35	105.98 $mA \cdot mg^{-1}$	In this work
	NSPd-SCO_{Ur}	0.32	1.0 M NaOH	Hg/HgO	−0.91	+0.02	286.12 $mA \cdot mg^{-1}$	−0.35	53.25 $mA \cdot mg^{-1}$	In this work
	NSPd	0.32	1.0 M NaOH	Hg/HgO	−0.99	−0.02	171.60 $mA \cdot mg^{-1}$	−0.39	16.06 $mA \cdot mg^{-1}$	In this work
Formaldehyde	Fe/FeZMCPE	0.13	1.0 M HCl	SCE	Un-R	+0.55	19.8 $mA \cdot cm^{-2}$	Un-R	Un-R	[2]
	Pt-SWNT/PANI	0.5	0.5 M $HClO_4$	SCE	+0.20	+0.62	0.08 $A \cdot cm^{-2}$	+0.49	0.95 $A \cdot cm^{-2}$	[45]
	Ni/P(NMA)MCPE	0.01	0.1 M NaOH	Ag/AgCl	Un-R	+0.60	1,000 μA	Un-R	Un-R	[4]
	NSPd-SCO_{Gl}	0.18	1.0 M NaOH	Hg/HgO	−1.00	+0.17	943.07 $mA \cdot mg^{-1}$	−0.31	388.13 $mA \cdot mg^{-1}$	In this work
	NSPd-SCO_{Ur}	0.18	1.0 M NaOH	Hg/HgO	−0.97	+0.16	364.27 $mA \cdot mg^{-1}$	−0.20	251.27 $mA \cdot mg^{-1}$	In this work
	NSPd	0.18	1.0 M NaOH	Hg/HgO	−0.95	−0.11	59.07 $mA \cdot mg^{-1}$	−0.49	−0.53 $mA \cdot mg^{-1}$	In this work
Formic acid	Pd/C	0.5	0.5 M H_2SO_4	Ag/AgCl	+0.037	+0.24	21.3 $mA \cdot cm^{-2}$	+0.24	10 $mA \cdot cm^{-2}$	[46]
	Pd-Co/G	0.5	0.5 M H_2SO_4	Ag/AgCl	−0.062	+0.20	151.32 $mA \cdot cm^{-2}$	+0.22	110 $mA \cdot cm^{-2}$	
	Pd_7Bi_1/C	0.5	0.5 M H_2SO_4	Ag/AgCl	+0.085	+0.1	15.8 $mA \cdot cm^{-2}$	+0.6	12.5 $mA \cdot cm^{-2}$	[47]
	NSPd-SCO_{Gl}	0.09	0.1 M H_2SO_4	SCE	−0.24	+0.22	329.87 $mA \cdot mg^{-1}$	+0.27	358.82 $mA \cdot mg^{-1}$	In this work
	NSPd-SCO_{Ur}	0.09	0.1 M H_2SO_4	SCE	−0.24	+0.33	285.72 $mA \cdot mg^{-1}$	+0.10	87.10 $mA \cdot mg^{-1}$	In this work
	NSPd	0.09	0.1 M H_2SO_4	SCE	−0.23	+0.17	55.69 $mA \cdot mg^{-1}$	+0.37	21.41 $mA \cdot mg^{-1}$	In this work

*Unreported

in Table 2. Based on Fig. 5, there are two oxidation peaks in each voltammogram. During the forward sweeping, the single-carbon molecules electrooxidation was conducted along to prepare an intermediate number on the surface of the working electrode. In the backward sweeping, the second oxidation peak appeared owing to the electrooxidation of intermediates. Table 2 reports the electrochemical quantities, as obtained from Fig. 5. Accordingly, the supported catalysts exposed a much higher mass current density (I) compared to the GC/NSPd electrode for the electrooxidation of all three molecules; that was due to higher NSPd resistance towards sintering, dissolution, and aggregation. Also, it was observed the higher current for electrooxidation of single-carbon molecules on GC/NSPd-SCO_{Gl} compared to GC/NSPd-SCO_{Ur} due to better dispersion and higher surface area of NSPd as the main component of electrocatalyst on SCO_{Gl} than SCO_{Ur}. However, a slight positive shift in the onset (E_{onset}), forward (E_f), and backward (E_b) peak potentials for NSPd-SCO_{Ur} electrode was often seen compared to the GC/NSPd-SCO_{Gl} electrode, which may be ascribed to preparing

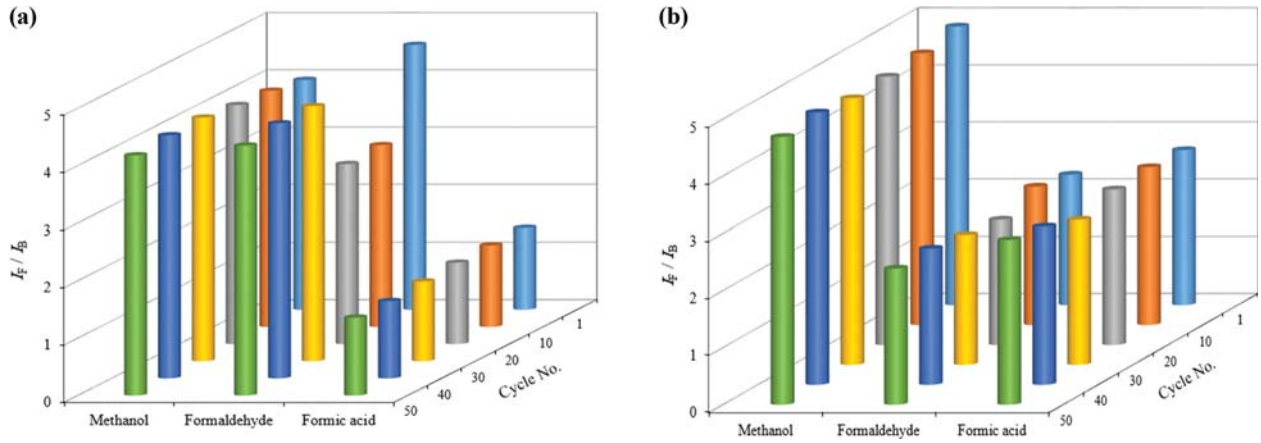

Fig. 6. I_F/I_B ratios as the function of cycle number for 0.80 M Methanol, 0.18 M Formaldehyde, and 0.51 M Formic acid, electrooxidation on (a) GC/NSPd-SCO_{GI} and (b) GC/NSPd-SCO_{Ur} electrodes.

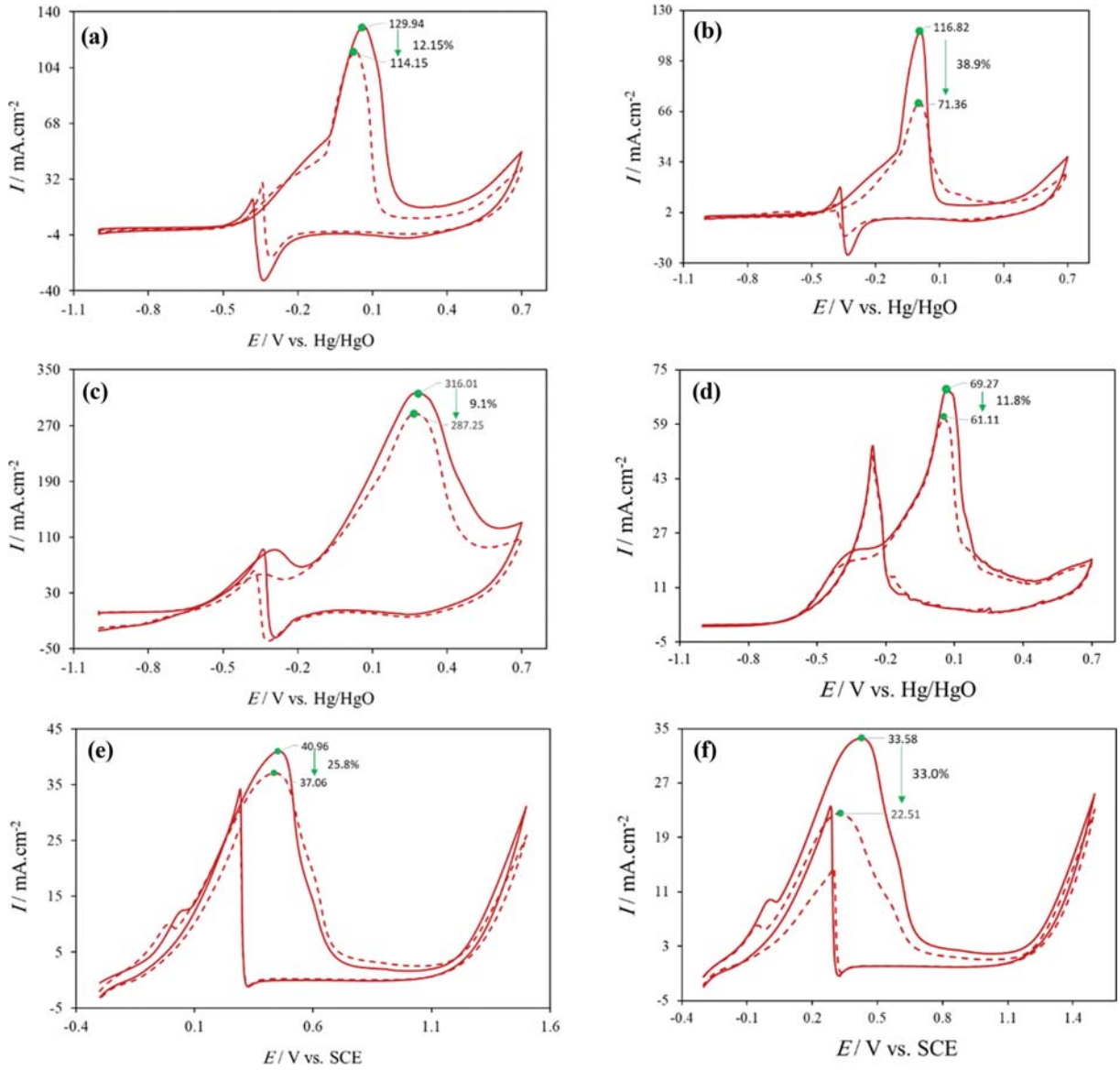

Fig. 7. The cycling stability of peak current densities after 100 runs for oxidation of ((a) and (b)) 0.80 M Methanol, ((c) and (d)) 0.18 M Formaldehyde, and ((e) and (f)) 0.51 M Formic acid on NSPd-SCO_{GI} and NSPd-SCO_{Ur} electrocatalysts, respectively.

more intermediate in the higher current. The results are comparable to some introduced catalysts in literature for electrooxidation of all three molecules [3,4,41-46] (see Table 2). This performance improvement can be for two reasons: Faster release of NSPd surface by intermediate species due to higher surface area and less accumulation of NSPd, and reduction of the mass transfer resistance due to the storage of oxidized species within the cavities of spongy support.

The cycling stability of the NSPd-SCO_{Gl} and NSPd-SCO_{Ur} was considered in order to study the poisoning influence of both modified electrodes during the electrooxidation of single-carbon molecules. Fig. 6 shows the ratios of the peak current at forward and backward sweeps (I_F/I_B) *vs.* cycle number towards 0.80 M methanol, 0.18 M formaldehyde, and 0.51 M formic acid electrooxidation on GC/NSPd-SCO_{Gl} and GC/NSPd-SCO_{Ur} electrodes. The I_F/I_B determined the electrocatalyst tolerance to accumulate carbonaceous intermediate. As observed, there is a slight decrease during a sequential scan. The percentage loss of efficiency was lower for GC/NSPd-SCO_{Gl} than GC/NSPd-SCO_{Ur} indicating higher NSPd resistance towards sintering, dissolution, and aggregation on SCO_{Gl} as more porous support. The prime reason for this result can be explained with the presence of holes in SCO_{Gl} in comparison to SCO_{Ur}. The nanocatalysts were held in these holes, which could diminish the sintering, dissolution, and aggregation of Pd.

The cycling stability of two electrocatalysts was examined towards electrooxidation of single-carbon molecules. The current densities of forward peaks for 1th and 100th cycles were recorded to calculate the decay percentages for NSPd-SCO_{Gl} and NSPd-SCO_{Ur}, as shown in Fig. 7. The NSPd-SCO_{Gl} electrocatalyst displays lesser decay of its initial activity compared to NSPd-SCO_{Ur} for electrooxidation of all three fuels after 100 runs. Thus, the NSPd-SCO_{Gl} represented more cycling stability than NSPd-SCO_{Ur}. So, SCO_{Gl}

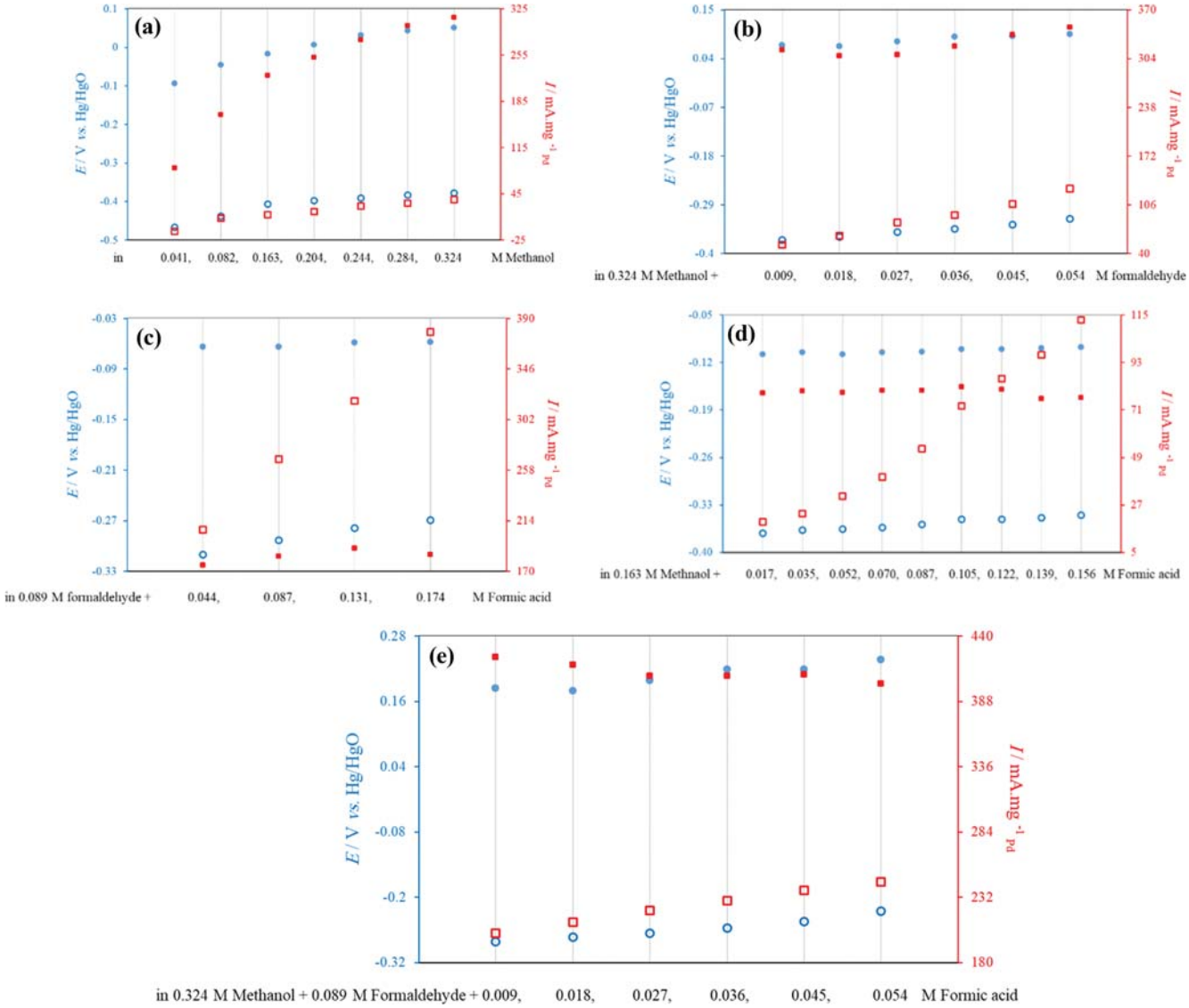

Fig. 8. The influence plots of concentration of electrooxidized species on current (□) and peak potential (○) at forward (filled) and backward (hollow) sweeping in 1 M NaOH containing increasing concentration: Methanol, Formaldehyde and Formic acid on GC/NSPd-SCO_{Ur} electrode with 0.05 V·s^{-1} sweep rate.

was a better support than SCO_{Ur} due to more porous structure. The palladium particles as main catalytic components were held in holes, which can reduce the sintering, dissolution, and aggregation of Pd.

3. Mechanism Proposal

For the first time, to study the electrooxidation mechanism of single-carbon molecules, the CV was used as an effective technique. Hence, the electrooxidation CVs on NSPd-SCO_{Ur} electrode containing increasing concentration of methanol (in absence of other species), formaldehyde (in constant methanol concentration), formic acid (in constant formaldehyde concentration), formic acid (in constant methanol concentration) and formic acid (in constant methanol and formaldehyde concentration) in 1 M NaOH were recorded and displayed in Fig. 8(a) through 8(e), respectively. Then, based on Fig. 8(a), it was seen that adding the methanol concentration up to 0.324 M increased the peak currents at forward and backward sweeps, while both peaks shifted toward the positive potentials. It can be attributed to NSPd poisoning by the adsorbed intermediates. According to Fig. 8(b), the formaldehyde addition to the electrolyte containing 0.324 M methanol did not affect the forward peak; nevertheless, the backward peak shifted toward the high current and positive potential. Such behavior was observed in the formic acid addition to the electrolyte containing 0.089 M formaldehyde (see Fig. 8(c)). As seen in Fig. 8(d), the formic acid addition to the electrolyte containing 0.163 M methanol, the current of two peaks at −0.27 and −0.34 V *vs.* Hg/HgO (in forward and backward sweeps, respectively) were increased, without any change at potential, while the oxidative peak at −0.1 V *vs.* Hg/HgO was approximately constant. Then based on Fig. 8(e), the formic acid addition to the electrolyte containing 0.324 M methanol and 0.089 M formaldehyde, the first peak at forward sweeping shifted toward the low current and positive potential, while the second peak at backward sweeping shifted toward the high current and positive potential. It confirmed the influence of each species on the intermediate electrooxidation of other species. Hence, it is probable that methanol electrooxidation can be followed by the production of formaldehyde and formic acid as intermediates. Thus, during electrooxidation reaction, a percentage of methanol (alcohol) molecules were converted to formaldehyde (aldehyde) and, in the following, to formic acid (carboxylic acid) before creation of CO_2 as the final production of complete electrooxidation. Our proposal was in agreement with the chromatographic study by Sequeira et al. [47]. Although, the result in Fig. 8(e) indicates that the direct conversion path of methanol to formic acid, cannot be entirely rejected.

CONCLUSION

Solution combustion synthesis is a suitable easy-eco, and the rapid route was employed to synthesize spongy ceria with two different fuels. The electrocatalytic performance of NSPd-SCO_{Gl} and NSPd-SCO_{Ur} toward electrooxidation of single-carbon molecules was considered *via* the techniques of CV and CA. According to the results, the performance of the modified electrodes increased in the order of non-supported palladium<NSPd-SCO_{Ur}<NSPd-SCO_{Gl}. The spongy structural network of SCO affected the electrochemical surface area, dispersion, and durability of NSPd. It also increased the capability of removing the poisoning species of the electrooxidation of single-carbon molecules through the lattice oxygen, and the creation of the oxidation-reduction cycle between the high and low chemical valents of cerium, leading to increase the NSPd performance. The electrooxidation mechanism of single-carbon molecules was evaluated by using the CV technique as follows: Alcohol→aldehyde→carboxylic acid before conversion to CO_2 as the final production of complete electrooxidation of single-carbon molecules. The cycling stability of two electrocatalysts confirmed higher NSPd resistance towards sintering, dissolution, and aggregation on SCO_{Gl} as more porous support than NSPd-SCO_{Ur}, which was the reason for the higher activity of GC/NSPd-SCO_{Gl} compared to GC/NSPd-SCO_{Ur}.

SUPPORTING INFORMATION

Additional information as noted in the text. This information is available via the Internet at http://www.springer.com/chemistry/journal/11814.

REFERENCES

1. J. B Raoof, R. Ojani and S. R. Hosseini, *Microchim. Acta*, **180**, 879 (2013).
2. M. Abrishamkar and M. Barootkoob, *Int. J. Hydrogen Energy*, **42**, 23821 (2017).
3. L. Feng, J. Chang, K. Jiang, H. Xue, Ch. Liu, W. B. Cai, W. Xing and J. Zhang, *Nano Energy*, **30**, 355 (2016).
4. J. B. Raoof, A. Omrani, R. Ojani and F. Monfared, *J. Electroanal. Chem*., **633**, 153 (2009).
5. D. Prasanna and V. Selvaraj, *Korean J. Chem. Eng*., **33**, 1489 (2016).
6. G. Sheng, J. Chen, H. Ye, Zh. Hu, X. Zh. Fu, R. Sun, W. Huang and Ch. P. Wong, *J. Colloid Interface Sci*., **522**, 264 (2018).
7. M Hepel, I Kumarihamy and C. J. Zhong, *Electrochem. Commun*., **8**, 1439 (2006).
8. Y. Zhang, Y. Liu, W. Liu, X. Li and L. Mao, *Appl. Surf. Sci*., **407**, 64 (2017).
9. D. Sebastián, M. J. Nieto-Monge, S. Pérez-Rodríguez, E. Pastor and M. J. Lázaro, *Energies*, **11**, 831 (2018).
10. G. Wang, K. Ye, J. Shao, Y. Zhang, K. Zhu, K. Cheng, J. Yan, G. Wang and D. Cao, *Int. J. Hydrogen Energy*, **43**, 9316 (2018).
11. B. Kuppan and P. Selvam, *Pro. Nat. Sci. Mater*., **22**, 616 (2012).
12. F. B. Zhang, J. X. Jiang and Y. Ni, *Mater. Sci. Eng. B*, **190**, 90 (2014).
13. S. Zhao, H. Yin, L. Du, G. Yin, Z. Tang and S. Liu, *J. Mater. Chem. A*, **2**, 3719 (2014).
14. H. A. Gasteiger, Sh. S. Kocha, B. Sompalli and F. T. Wagner, *Appl. Catal. B*, **56**, 9 (2005).
15. M. Zahed, M. Shafiee Afarani and D. Mohebbi-Kalhori, *Appl. Phys. A. Mater*., **120**, 215 (2015).
16. P. J. Kulesza, B. Grzybowska, M. A. Malik, M. Chojak and K. Miecznikowski, *J. Electroanal. Chem*., **512**, 110 (2001).
17. J. M. Macak, P. J. Barczuk, H. Tsuchiya, M. Z. Nowakowska, A. Ghicov, M. Chojak, S. Bauer, S. Virtanen, P. J. Kulesza and P. Schmuki, *Electrochem. Commun*., **7**, 1417 (2005).
18. M. S. Saha, R. Li and X. Sun, *Electrochem. Commun*., **9**, 2229 (2007).
19. M. A. Hoque, D. C. Higgins, F. M. Hassan, J. Y. Choi, M. D. Pritzker and Zh. Chen, *Electrochim. Acta*, **121**, 421 (2014).

20. G. S. Chai, I. S. Shin and J. S. Yu, *Adv. Mater.*, **16**, 2057 (2004).
21. Zh. Cui, M. Yang and F. J. Di-Salvo, *ACS Nano*, **8**, 6106 (2014).
22. J. Zhan, M. Cai, Ch. Zhang and Ch. Wang, *Electrochim. Acta*, **154**, 70 (2015).
23. B. Bai, J. Li and J. Hao, *Appl. Catal. B*, **164**, 241 (2015).
24. X. Xie, Y. Li, Zh. Q. Liu, M. Haruta and W. Shen, *Nature*, **458**, 746 (2009).
25. L. Hu, Q. Peng and Y. Li, *J. Am. Chem. Soc.*, **130**, 16136 (2008).
26. J. B. Wu, Z. G. Li, X. H. Huang and Y. Lin, *J. Power Sources*, **224**, 1 (2013).
27. D. Delimaris and Th. Ioannides, *Appl. Catal. B*, **84**, 303 (2008).
28. A. Abad, P. Concepción, A. Corma and H. García, *Angew. Chem.*, **44**, 4066 (2005).
29. H. Ma, L. Zeng, H. Tian, D. Li, X. Wang, X. Li and J. Gong, *Appl. Catal. B*, **181**, 321 (2016).
30. S. A. Hassanzadeh-Tabrizi, M. Mazaheri, M. Aminzare and S. K. Sadrnezhaad, *J. Alloys Compd.*, **491**, 499 (2010).
31. T. Mokkelbost, I. Kaus, T. Grande and M. A. Einarsrud, *Chem. Mater.*, **16**, 5489 (2004).
32. T. Yu, J. Joo, Y. I. Park and T. Hyeon, *Angew. Chem.*, **117**, 7577 (2005).
33. L. Yan, R. Yu, J. Chen and X. Xing, *Cryst. Growth Des.*, **8**, 1474 (2008).
34. J. Liu, D. Zhang, X. Pu, J. Liu and R. Zhang, *Mater. Lett.*, **117**, 158 (2014).
35. Z. Yavari, M. Noroozifar and M. Khorasani-Motlagh, *J. Appl. Electrochem.*, **45**, 439 (2015).
36. L. M. Proniewicz, C. Paluszkiewicz, A. Wesełucha-Birczyńska, H. Majcherczyk, A. Barański and A. Konieczna, *J. Mol. Struct.*, **596**, 163 (2001).
37. M. Manivannan, *Int. J. Eng. Sci. Technol.*, **3**, 8048 (2011).
38. R. N. Singh, T. Sharma, A. Singh, Anindita, D. Mishra and S. K. Tiwari, *Electrochim. Acta*, **53**, 2322 (2008).
39. L. Li and Y. Xing, *Energies*, **2**, 789 (2009).
40. F. M. Toma, A. Sartorel, M. Iurlo, M. Carraro, P. Parisse, Ch. Maccato, S. Rapino, B. R. Gonzalez, H. Amenitsch, T. D. Ros, L. Casalis, A. Goldoni, M. Marcaccio, G. Scorrano, G. Scoles, F. Paolucci, M. Prato and M. Bonchio, *Nat. Chem.*, **2**, 826 (2010).
41. Y. Zhao, L. Fan, J. Ren and B. Hong, *Int. J. Hydrogen Energy*, **39**, 4544 (2014).
42. Zh. Fu, W. Li, W. Zhang, F. Sun, Zh. Zhou and X. Xiang, *Int. J. Hydrogen Energy*, **35**, 8101 (2010).
43. M. Noroozifar, Z. Yavari, M. Khorasani-Motlagh, T. Ghasemi, S. H. Rohani-Yazdi and M. Mohammadi, *RSC Adv.*, **6**, 563 (2016).
44. Zh. Wang, Z. Zhu, J. Shi and H. L. Li, *Appl. Surf. Sci.*, **253**, 8811 (2007).
45. A. Shafaei Douk, H. Saravani and M. Noroozifar, *J. Alloys Compd.*, **739**, 882 (2018).
46. S. Yang, J. Yang, Y. Chung and Y. Kwon, *Int. J. Hydrogen Energy*, **42**, 17211 (2017).
47. C. A. C. Sequeira, D. M. F. Santos and P. S. D. Brito, *Appl. Surf. Sci.*, **252**, 6093 (2006).

Supporting Information

Electrooxidation of single-carbon molecules by nanostructured Pd-decorated spongy ceria

Zahra Yavari[*,,†], Mahdi Shafiee Afarani[***], Amir Masoud Arabi[****], and Meissam Noroozifar[*****,†]**

*Department of Chemistry, University of Sistan and Baluchestan, P.O. Box 98135-674, Zahedan, Iran
**Renewable Energies Research Institute, University of Sistan and Baluchestan, Zahedan, Iran
***Department of Materials Engineering, Faculty of Engineering, University of Sistan and Baluchestan, Zahedan, Iran
****Department of Inorganic Pigments and Glazes, Institute for Color Science and Technology (ICST), Tehran, Iran
*****Department of Physical and Environmental Sciences, University of Toronto Scarborough 1265 Military Trail, Toronto, Ontario, M1C 1A4, Canada

(*Received 24 December 2019 • Revised 9 May 2020 • Accepted 11 May 2020*)

To show the potential applications of the NSPd-SCO_{Gl} and NSPd-SCO_{Ur}, the electrochemical properties of the two samples were considered in alkali (corresponding to the alkaline fuel cell). Electrochemical examinations of the as-modified GC/NSPd-SCO_{Gl} and GC/NSPd-SCO_{Ur} electrodes were conducted by using cyclic voltammograms (CV) plots at −1.0 to +0.7 V *vs.* Hg/HgO (Fig. S1(a)).

It was seen that the voltammogram of GC/NSPd-SCO_{Gl} and GC/NSPd-SCO_{Ur} electrodes reveals the characteristics of Pd metal [1,2]. The forward sweeping directed an electrooxidation reaction on the electrode surface, resulting in the creation of Pd oxides (+0.3 to +0.7 V *vs.* Hg/HgO) and hydrogen desorption (−1.0 to −0.3 V *vs.* Hg/HgO), while the backward sweep reflected the reduction of the Pd oxides (−0.1 to −0.6 V *vs.* Hg/HgO) and hydrogen adsorption (−0.7 to −1.0 V *vs.* Hg/HgO). The potential region of −0.3 to +0.3 V *vs.* Hg/HgO and −0.7 to +0.1 V *vs.* Hg/HgO in forward and backward sweeps were respectively related to double layer on the working electrode. The coulombic charge (Q) for Pd oxides reduction and hydrogen adsorption/desorption is gotten *via* an integral of the own peak, that is commonly used to determine the electrochemical active surface area (EAS) of the modified electrodes ac-

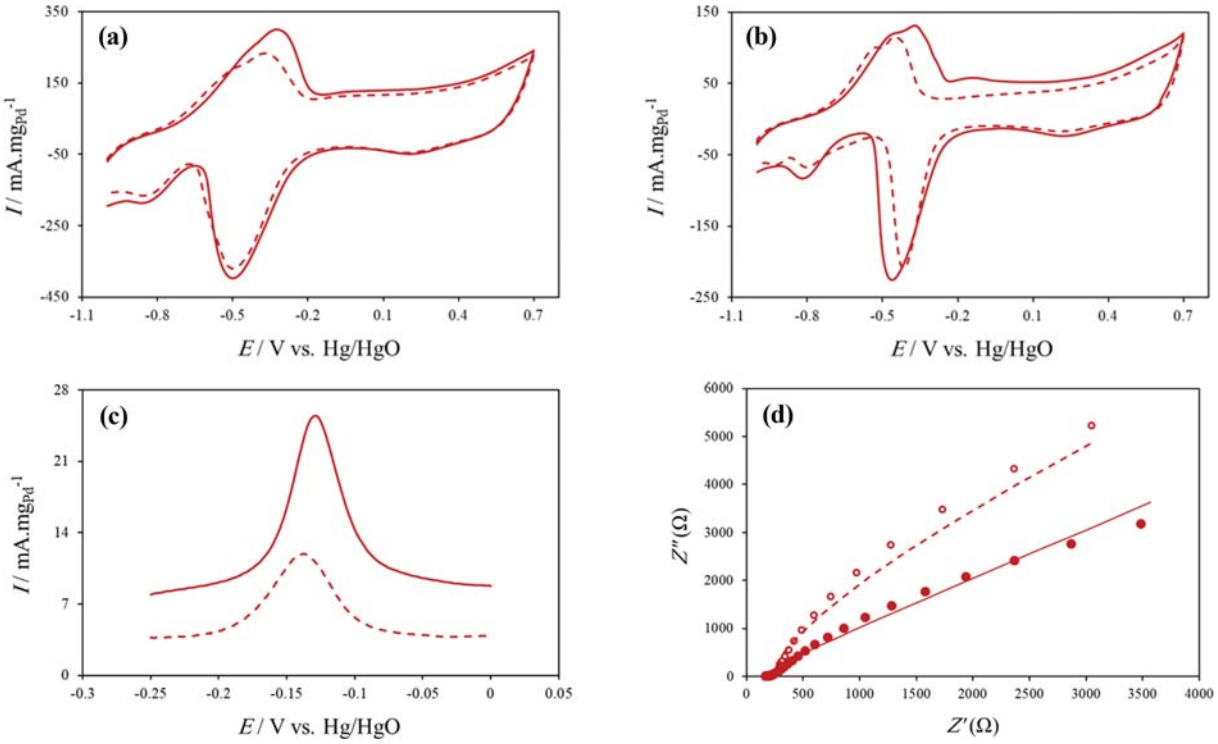

Fig. S1. Voltammograms of (a) 1th and (b) 1,000th cycles, and (c) CO stripping in 1 M NaOH at 0.05 V·s^{-1} sweep rate and (d) Nyquist plots recorded at potential of 0.30 V non-fitted (dots) and fitted (line) for (—) GC/NSPd-SCO_{Gl} and (----) GC/NSPd-SCO_{Ur} electrodes with NSPd loading of 0.236 mg·cm^{-2}.

cording to [15] (See Table S1) to assess the electrocatalytic efficiency of NSPd-SCO_{Gl} and NSPd-SCO_{Ur}. The NSPd dispersion (D_{Pd}) on both supports was achieved according to [S4] (See Table S1). For more investigation, accelerated durability test (ADT) of the modified electrodes was tested with applying potentials −1.0 to +0.7 V *vs.* Hg/HgO after 1,000 potential runs, continuously; that cyclic voltammograms (CV) and EAS loss percentages for both modified electrodes are represented as Fig. S1(b), and Table S1. The D_{Pd} dropped after ADT for the electrocatalysts, representative a notable dawn fall for EAS with sintering, dissolution, and aggregation of NSPd particles. The investigation of data showed that utilizing more spongy support enhanced the EAS, and D of NSPd; so that NSPd-SCO_{Gl} exhibited a superior dispersion and stability than NSPd-SCO_{Ur}. The better EAS of NSPd-SCO_{Gl} and NSPd-SCO_{Ur} electrocatalysts in comparison to other Pd-containing catalysts [5-7] is attributed to the synergistic influence of ceria support and proper distribution of NSPd.

To investigate CO stripping, the linear voltammograms between −0.25 and +0.00 V *vs.* Hg/HgO were recorded and represented in Fig. S1(c) for both modified electrodes. The mass current density of the CO peak for GC/NSPd-SCO_{Gl} (25.44 mA·mg^{-1}) was more than GC/NSPd-SCO_{Ur} (11.89 mA·mg^{-1}). The peak potential at GC/NSPd-SCO_{Gl} (−0.13 V *vs.* Hg/HgO) shifted by 0.01 V to the negative direction compared with that GC/NSPd-SCO_{Ur} (−0.14 V *vs.* Hg/HgO).

The based on Table S1, the $Q_{CO_{ads}}$ was 3.04 and 1.38 mC·cm^{-2} for GC/NSPd-SCO_{Gl} and GC/NSPd-SCO_{Ur}, respectively. This difference is recognized to the CO removal on the NSPd surface through the higher surface area. The roughness (r_f, dimensionless) and mass-specific surface area (A, m^2·g$^{-1}{}_{Pd}$) from CO stripping were calculated with [S8] (See Table S1). The comparison of obtained surface area from Q_H, Q_{Pd}, and Q_{CO} indicated acceptable agreement for both modified electrodes.

The EIS technique was used to examine the capacitance of the mentioned catalyst layers on modified electrodes; that it can be related to electrocatalyst active area. The Nyquist plots of NSPd-SCO_{Gl} and NSPd-SCO_{Ur} electrocatalysts are displayed in Fig. S1(d). The Nyquist profiles demonstrated that a process of charge transfer occurred on the surface of both modified electrodes. A semicircle with a smaller diameter is because of a less resistance of charge transfer (R_{CT}) and a quicker charge transfer process [S9]. The exchange current (I_0) for both electrocatalysts were measured by using R_{CT} (See Table S1). The less R_{CT} and high I_0 values compared to [10,11] represented superior electrocatalytic performance on GC/NSPd-SCO_{Gl} and GC/NSPd-SCO_{Ur}; because of the porous S1(d) structures of NSPd-SCO_{Gl} and NSPd-SCO_{Ur} make possible the quick flow of electron transportation.

The electrooxidation reaction was tested on the modified electrodes under the variable conditions: concentration of electrooxidized species, sweep rate, and temperature; while the parameters as estimated from corresponding CVs were expressed as Table S2.

The effect of adding the concentration of electrooxidized specie was determined on the potential and the current of electrooxidation reaction at positive and negative sweeps on GC/NSPd-SCO_{Gl} and GC/NSPd-SCO_{Ur} electrodes in 1 M NaOH at −1 to +0.7 V *vs.* Hg/HgO the potential range and 0.05 V·s^{-1} sweep rate for methanol and formaldehyde. The 0.1 M H_2SO_4 solution, −0.3 to +1.5 V *vs.* SCE and 0.05 V·s^{-1} were the electrolyte, potential range and sweep rate for formic acid, respectively. According to Fig. S2, the density current was increased with increasing concentration of electrooxidized specie. However, it did not have any significant increase in concentrations more than a known concentration for every species due to the occupation of active sites and it was in more concentration for the electrooxidation on GC/NSPd-SCO_{Gl} than GC/

Table S1. The calculated results from voltammograms (after 1 and 1,000 cycles), CO-stripping at 0.05 V·s^{-1} sweep rate and Nyquist curves of modified electrodes

Electrode	GC/NSPd-SCO_{Gl}		GC/NSPd-SCO_{Ur}	
	1th cycle	1,000th cycle	1th cycle	1,000th cycle
Q'_H (mC·cm^{-2})	252.81	96.57	211.52	73.11
Q''_H (mC·cm^{-2})	119.22	50.78	101.01	51.86
$Q_H{}^a$ (mC·cm^{-2})	186.01	73.68	156.27	62.49
$EAS_H{}^b$ (m^2·g^{-1})	187.66	74.33	157.65	63.04
$D_{Pd}{}^c \times 10^{-2}$	13.47	5.34	11.31	4.53
% $lossADT_H{}^d$	60.39		60.02	
Q_{pd} (mC·cm^{-2})	258.85	107.51	242.45	70.50
$EAS_{Pd}{}^e$ (m^2·g^{-1})	270.82	112.48	253.66	73.76
% $lossADT_{Pd}{}^f$	58.47		70.92	
$Q_{CO_{ads}}$ (mC·cm^{-2})	3.04		1.38	
$r_f{}^g{}_{dimensionless}$	7.24		3.29	
A^h (m^2·g$^{-1}{}_{Pd}$)	3.07		1.39	
R_{CT} (μΩ)	2.14		15.90	
$I_0{}^i$ (A)	12.00		1.61	

[a] $Q_H = \frac{Q'_H + Q''_H}{2}$ {electrochemically desorption (Q'_H) and adsorption (Q''_H) of H_2 molecules on the NSPd sites}

[b] $EAS_H = \frac{Q_H}{C \times l_{Pd}}$ {C=0.420 mC·cm^{-2} and l_{Pd}=0.236 mg·cm^{-2}}

[c] $D_{Pd} = \frac{EAS_H}{\frac{1}{M_{Pd}} \times (N_A \times S_{Pd})}$ {M_{Pd}=Molecular weight (106.42 g·mol^{-1}), N_A= Avogadro number and S_{Pd}=atomic surface area (24.63×10^{-20} m^2)}

[d] $\%loss_{ADT_H} = \frac{(EAS_{H_{1^{th}\,cycle}} - EAS_{H_{1000^{th}\,cycle}})}{EAS_{H_{1^{th}\,cycle}}} \times 100$

[e] $EAS_{Pd} = \frac{Q_{Pd}}{C \times l_{Pd}}$ {C=0.405 mC·cm^{-2} and l_{Pd}=0.236 mg·cm^{-2}}

[f] $\%loss_{ADT_{Pd}} = \frac{(EAS_{Pd_{1^{th}\,cycle}} - EAS_{Pd_{1000^{th}\,cycle}})}{EAS_{Pd_{1^{th}\,cycle}}} \times 100$

[g] $r_f = \frac{Q_{CO_{ads}}}{C}$ {C=0.420 mC·cm^{-2}}

[h] $A = \frac{r_f}{l_{Pd}}$ {l_{Pd}=0.236 mg·cm^{-2}}

[i] $I_0 = \frac{R \times T}{n \times F \times R_{CT}}$ {R=gas constant, T=absolute temperature, n=the number of transferred electrons (n=1), F=Faraday constant}

NSPd-SCO_{Ur} electrode. According to [S12], the slope of the current logarithm of the peak (log I) *vs.* the logarithm of concentration (log C) gives the reaction order concerning the initial concentration. It can seem as a result that reaction order at backward sweeping is more than forward sweeping.

The temperature effect at the electrochemical tests on the electrocatalytic activity of GC/NSPd-SCO_{Gl} and GC/NSPd-SCO_{Ur} electrodes toward the electrooxidation of single-carbon molecules was investigated by CV technique using different temperatures between 20 and 50 °C. The results presented that the enhancing temperature increased the current. At the same concentration, the higher current designated that the spongy structure of electrocatalyst possesses extra accessible active sites to participate in the electrooxidation of single-carbon molecules. The fitted line slope of Arrhenius plots {the natural logarithm of current (ln I_p) *vs.* the temperature reciprocal (T^{-1})} represented the activation energy with using the employing equation in [13]. It can be remarkable that of formaldehyde electrooxidation reaction had the least activation energy; which indicates its oxidation more convenient.

The CV curves of electrooxidation on GC/NSPd-SCO_{Gl} and GC/NSPd-SCO_{Ur} electrodes were recorded in a certain concentration at various sweeping rates (υ) between 0.01 and 0.10 $V{\cdot}s^{-1}$. It was seen that the peak current and potential of electrooxidation were increased by increasing the scanning rate. The slope of the peak potential *vs.* ln (υ) and the anodic peak current of electrooxidation reactions *vs.* the square root of the sweeping rate ($\upsilon^{1/2}$) are explained in Table 4. The electron transfer and diffusion coefficients were calculated according to [14] and [15] (See Table S2); respectively.

Table S2. The investigation results of influence of SOM concentration, temperature and scan rate on the SOMs electroxidation

Electrode		Reaction order[a]		E_a [b] ($kJ.mol^{-1}$)		$\delta E_f/\delta \ln \upsilon$	$\delta J_f/\delta \upsilon^{1/2}$	α[c]	C ($mol{\cdot}cm^{-3}$)	n*	D[d]* ($cm^2{\cdot}s^{-1}$)
		Forward sweep	Backward sweep	Forward sweep	Backward sweep						
GC/NSPd-SCO_{Gl}	Methanol	0.32 ($R^{2\#}$=0.998)	2.37 (R^2=0.910)	6.39 (s^+=–768.85 & R^2=0.918)	15.46 (s=–1859.70 & R^2=0.925)	0.11 (R^2=0.995)	618.08 (R^2=0.953)	0.96	800	6	3.17×10^{-5}
	Formaldehyde	0.42 (R^2=0.914)	2.62 (R^2=0.920)	7.48 (s=–899.88 & R^2=0.906)	33.08 (s=–3978.44 & R^2=0.953)	0.11 (R^2=0.976)	777.00 (R^2=0.987)	0.94	180	4	3.40×10^{-3}
	Formic acid	0.43 (R^2=0.926)	0.29 (R^2=0.900)	20.14 (s=–2421.82 & R^2=0.924)	17.36 (s=–2087.90 & R^2=0.928)	0.09 (R^2=0.931)	99.51 (R^2=0.985)	0.86	510	2	6.14×10^{-5}
GC/NSPd-SCO_{Ur}	Methanol	0.59 (R^2=0.949)	1.03 (R^2=0.964)	20.20 (s=–2429.10 & R^2=0.916)	30.69 (s=–3691.64 & R^2=0.931)	0.02 (R^2=0.997)	23.47 (R^2=0.945)	0.75	800	6	5.85×10^{-8}
	Formaldehyde	0.59 (R^2=0.989)	1.08 (R^2=0.977)	4.00 (s=–481.23 & R^2=0.972)	13.92 (s=–1673.70 & R^2=0.952)	0.10 (R^2=0.996)	316.52 (R^2=0.996)	0.94	180	4	5.68×10^{-4}
	Formic acid	0.32 (R^2=0.958)	1.90 (R^2=0.936)	9.08 (s=–1092.42 & R^2=0.900)	11.78 (s=–1417.41 & R^2=0.977)	0.15 (R^2=0.947)	269.07 (R^2=0.986)	0.92	510	2	4.19×10^{-4}

[a] $\log I = n \log C + B$ {n=reaction order, C=concentration and B=interception}

[b] $s = \dfrac{\delta \ln I_p}{\delta\left(\frac{1}{T}\right)} = \dfrac{-E_a}{R}$ {E_a=activation energy and R=gas constant}

[c] $\alpha = 1 - \dfrac{R\times T}{\frac{\delta E_p}{\delta(\ln \upsilon)}\times n\times F}$ {α=electron transfer coefficient, υ=scan rate, R=gas constant, T=293 K, F=Faraday constant and n=electrons number transferred during oxidation of one mol of specie}

[d] $D = \dfrac{\left(\frac{\delta J_P}{\delta \upsilon^{1/2}}\right)^2 \times R\times T}{2.46\times10^{-7}\times(n\times F)^3\times\alpha\times C^2}$ {D=diffusion coefficient and C=concentration}

*If the oxidation reaction be complete (to produce CO_2), and not partial oxidation.

#R-squared in linear fitting.

+Slop of fitted line.

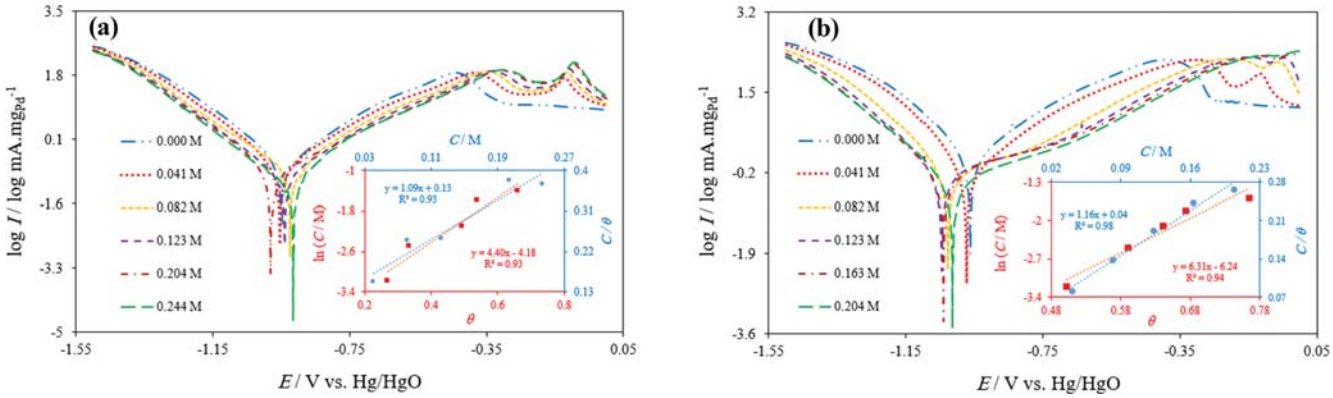

Fig. S2. Tafel curves for (a) GC/PdNPs-CeO_{2Gl}MP and (b) GC/PdNPs-CeO_{2Ur}MP electrodes in 1 M NaOH at different SOM-1 concentration with 0.05 V·s^{-1} scan rate; Inset: The linear results fitting for (□) Temkin and (○) Langmuir isotherms.

The linearity of the relationship between I–$\upsilon^{1/2}$ and E–ln (υ) referred to the mass transport as control process and an irreversible charge transfer process for the overall electrooxidation, respectively.

The adsorption of single-carbon molecules on the electrocatalysts surface is a substitution process between electrooxidized species in the aqueous phase and H_2O molecules which adsorbed on the surface of the electrocatalysts. The main adsorption types to describe the heterogeneous electrocatalysis are the physical and chemical adsorptions; while can be determined *via* isotherms like Temkin: $\ln C = -\ln K + a\theta$ and Langmuir: $\frac{C}{\theta} = \frac{1}{K} + C$; while C is concentration of electrooxidized specie; K is the constant of adsorption equilibrium, and the degree of surface coverage was calculated as $\theta = 1 - \frac{I_{in\ presence\ of\ electrooxidized\ specie}}{I_{in\ absence\ of\ electrooxidized\ specie}}$ [6]. Hence, the potentiodynamic polarization (Tafel curves) of electrooxidation reaction on GC/NSPd-SCO_{Gl} and GC/NSPd-SCO_{Ur} electrodes were analyzed in 1 M NaOH at different methanol concentrations with 0.05 V·s^{-1} scan rate (Fig. S2) and in the following, the plots were made to fit the values to the two mentioned isotherms (Inset Fig. S2).

The good results fitting to both isotherms confirmed the validity of the proposed study to evaluate the methanol adsorption on the surface of the modified electrode. It was approved that the initial step in methanol electrooxidation included the methanol molecule adsorption following the Temkin isotherm [17], which remarks the interaction between the adsorbed species and that the adsorption energy losses linearly with the coverage. Such an approach appears more accurate than the Langmuir isotherm, which does not remark the interactions between the several species created during the electrooxidation [18].

REFERENCES

1. R. N. Singh, A. Singh and Anindita, *Carbon*, **47**, 271 (2009).
2. M. Wang, W. Liu and Ch. Huang, *Int. J. Hydrogen Energy*, **34**, 2758 (2009).
3. Z. Yavari, M. Noroozifar and T. Parvizi, *Environ. Prog. Sustain. Energy*, **37**, 597 (2018).
4. M. Noroozifar, Z. Yavari, M. Khorasani-Motlagh, T. Ghasemi, S. H. Rohani-Yazdi and M. Mohammadi, *RSC Adv.*, **6**, 563 (2016).
5. G. Sheng, J. Chen, H. Ye, Zh. Hu, X. Zh. Fu, R. Sun, W. Huang and Ch. P. Wong, *J. Colloid Interface Sci.*, **522**, 264 (2018).
6. Ch. Zhu, Q. Shi, Sh. Fu, J. Song, H. Xia, D. Du and Y. Lin, *Adv. Mater.*, **28**, 8779 (2016).
7. X. Qiu, H. Zhang, P. Wu, F. Zhang, S. Wei, D. Sun, L. Xu and Y. Tang, *Adv. Funct. Mater.*, **27**, 1603852 (2017).
8. J. M. Macak, P. J. Barczuk, H. Tsuchiya, M. Z. Nowakowska, A. Ghicov, M. Chojak, S. Bauer, S. Virtanen, P. J. Kulesza and P. Schmuki, *Electrochem. Commun.*, **7**, 1417 (2005).
9. H. Chen, Y. Huang, D. Tang, T. Zhang and Y. Wang, *Electrochim. Acta*, **158**, 18 (2015).
10. M. Zareie Yazdan-Abad, M. Noroozifar, A. R. Modaresi Alam and H. Saravani, *J. Mater. Chem. A*, **5**, 10244 (2017).
11. A. Shafaei Douk, H. Saravani and M. Noroozifar, *Int. J. Hydrogen Energy*, **42**, 15149 (2017).
12. Z. Yavari, M. Noroozifar and M. Khorasani-Motlagh, *J. Appl. Electrochem.*, **45**, 439 (2015).
13. S. Haghnegahdar and M. Noroozifar, *Electroanalysis*, **29**, 1 (2017).
14. Z. Yavari, M. Noroozifar and M. Khorasani-Motlagh, *J. Exp. Nanosci.*, **11**, 798 (2016).
15. D. J. Guo and H. L. Li, *J. Power Sources*, **160**, 44 (2006).
16. M. Dehdab, Z. Yavari, M. Darijani and A. Bargahi, *Desalination*, **400**, 7 (2016).
17. O. A. Khazova, A. Mikhailova, A. M. Skundin, E. K. Tuseeva, A. Havránek and K. Wippermann, *Fuel Cells*, **2**, 99 (2002).
18. A. Velázquez-Palenzuela, F. Centellas, J. A. Garrido, C. Arias, M. R. Rodríguez, E. Brillas and P. L. Cabot, *J. Power Sources*, **196**, 3503 (2011).